# *crossveinless-c* is a RhoGAP required for actin reorganisation during morphogenesis

**Barry Denholm[1], Stephen Brown[1,2], Robert P. Ray[3], Mar Ruiz-Gómez[4], Helen Skaer[1,*] and James Castelli-Gair Hombría[1,5]**

[1]Department of Zoology, University of Cambridge, Downing Street, Cambridge CB2 3EJ, UK
[2]Faculty of Life Sciences, University of Manchester, Michael Smith Building, Oxford Road, Manchester M13 9PT, UK
[3]School of Life Sciences, University of Sussex, Falmer, Brighton BN1 9QG, UK
[4]Facultad de Ciencias, Centro de Biologia Molecular, 'Severo Ochoa', CSIC-UAM, Cantoblanco, Madrid 28049, Spain
[5]Centro Andaluz de Biología del Desarrollo,Universidad Pablo de Olavide, Carretera de Utrera, Km 1, Sevilla 41013, Spain
*Author for correspondence (e-mail: hs17@cam.ac.uk)

*Accepted 18 March 2005*

Development 132, 2389-2400
Published by The Company of Biologists 2005
doi:10.1242/dev.01829

## Summary

**Members of the Rho family of small GTPases are required for many of the morphogenetic processes required to shape the animal body. The activity of this family is regulated in part by a class of proteins known as RhoGTPase Activating Proteins (RhoGAPs) that catalyse the conversion of RhoGTPases to their inactive state. In our search for genes that regulate *Drosophila* morphogenesis, we have isolated several lethal alleles of *crossveinless-c* (*cv-c*). Molecular characterisation reveals that *cv-c* encodes the RhoGAP protein RhoGAP88C. During embryonic development, *cv-c* is expressed in tissues undergoing morphogenetic movements; phenotypic analysis of the mutants reveals defects in the morphogenesis of these tissues. Genetic interactions between *cv-c* and RhoGTPase mutants indicate that Rho1, Rac1 and Rac2 are substrates for Cv-c, and suggest that the substrate specificity might be regulated in a tissue-dependent manner. In the absence of *cv-c* activity, tubulogenesis in the renal or Malpighian tubules fails and they collapse into a cyst-like sack. Further analysis of the role of *cv-c* in the Malpighian tubules demonstrates that its activity is required to regulate the re-organisation of the actin cytoskeleton during the process of convergent extension. In addition, overexpression of *cv-c* in the developing tubules gives rise to actin-associated membrane extensions. Thus, Cv-c function is required in tissues actively undergoing morphogenesis, and we propose that its role is to regulate RhoGTPase activity to promote the coordinated organisation of the actin cytoskeleton, possibly by stabilising plasma membrane/actin cytoskeleton interactions.**

Key words: *crossveinless-c*, *Drosophila*, Morphogenesis, RhoGTPase, RhoGAP, Actin cytoskeleton, Convergent extension

## Introduction

Morphogenesis describes a complex set of cell behaviours by which a tissue is formed; these include changes in cell shape, cell rearrangement and coordinated cell movement. Experimental evidence gathered over the past 15 years shows that the Rho family of small GTPases, which include the Rho, Rac and Cdc42 proteins, are central to the regulation of these processes (reviewed by Settleman, 2001; Van Aelst and Symons, 2002). Although this protein family has pleiotropic roles in diverse cellular and developmental contexts (Etienne-Manneville and Hall, 2002; Settleman, 2001), a commonality in their function is in the regulation of the cytoskeleton, particularly the actin cytoskeleton (Hall, 1998; Nobes and Hall, 1995a; Nobes and Hall, 1995b).

The Rho GTPase family of proteins act as 'molecular switches' that cycle between two conformational states, a GTP-bound state in which they are active and a GDP-bound inactive state. The balance between these states is controlled principally by two classes of regulatory proteins: the guanine nucleotide exchange factors (GEFs) that promote the active state by facilitating the release of GDP and subsequent rebinding of GTP; and the GTPase activating proteins (GAPs) that promote the inactive state by catalysing the weak intrinsic GTP hydrolysing capacity of the GTPase, thereby converting it to the inactive form. In many cases, it is crucial that the correct balance between these two states is properly regulated. This is evident in cases in which they are not, as deregulated GTPases can have catastrophic developmental consequences and can lead to cellular pathologies such as cancer (Boettner and Van Aelst, 2002; Jaffe and Hall, 2002).

In all animal genomes sequenced to date, there are considerably more genes encoding for GAPs and GEFs than the GTPases they regulate. For example, the human genome encodes ~20 Rho-family GTPases, but in excess of 50 different GAPs and GEFs (Bernards, 2003; Peck et al., 2002); similarly, the *Drosophila* genome encodes seven Rho-family GTPases but 21 GAPs and 20 GEFs (Bernards, 2003). The preponderance of GAPs and GEFs probably reflects the importance of controlling the activity of RhoGTPase family members. The 21 GAP proteins in *Drosophila* show considerable diversity in their domain architecture and this may provide context specificity for the multitude of functions

and outcomes of GTPase signalling. Although much is known about the catalytic function of the GAPs and GEFs, relatively little is known about how they function in a cellular or developmental context, e.g. their spatial and temporal regulation and the factors that control their specificity. Of the 21 *Drosophila* RhoGAPs, five have been studied to date (Billuart et al., 2001; Guichard et al., 1997; Lundström et al., 2004; Raymond et al., 2001; Sagnier et al., 2000; Sotillos and Campuzano, 2000). In most cases, these studies have used either gain-of-function analyses or dominant-negative approaches; therefore, the phenotypic defects in mutants have not been analysed.

We present evidence that viable alleles in the *crossveinless-c* (*cv-c*) gene are hypomorphic alleles of the RhoGAP88C gene. Three *cv-c* alleles have been described previously. These alleles are characterised by partial or complete loss of the posterior crossvein (PCV) and variable detachment of the anterior crossvein (ACV) in the wing (Fig. 1A) (Diaz-Benjumea, 1990; Edmondson, 1952; Stern, 1934). Despite having been first described over 70 years ago (Stern, 1934) and used as a marker for recombination studies, the molecular nature of the locus has until now remained a mystery.

We have generated lethal alleles of *cv-c*, and phenotypic analyses of these show that *cv-c* is required in the embryo in multiple tissues undergoing morphogenesis including the Malpighian tubules (MpTs), midgut, head, posterior spiracles and the epidermis during dorsal closure. We have chosen the MpTs to examine the loss- and gain-of-function *cv-c* phenotypes in more detail and find that Cv-c is autonomously required to regulate actin cytoskeleton dynamics during morphogenesis, and possibly in stabilising links between the cytoskeleton and the plasma membrane. In addition, genetic interactions between *cv-c* and RhoGTPase mutants show that Cv-c has specificity towards Rho, Rac1 and Rac2, and that it might regulate these GTPases in a tissue-specific manner. Our data therefore suggest that *cv-c* acts to ensure coordinated assembly of the actin cytoskeleton in many tissues undergoing morphogenesis by regulating the activity of specific RhoGTPases.

## Materials and methods

### Fly husbandry and stocks

All flies were cultured on standard media at 25°C. The following alleles were used for genetic interaction analysis: $Rho1^{72R}$, $Rac1^{J11}$, $Rac2^{\Delta}$, $Mtl^{A}$, $cdc42^{1}$, $cdc42^{2}$ and $cdc42^{4}$. For the RNAi experiments, the UAS-RhoGAP88C-dsRNA (Billuart et al., 2001) was crossed to the driver lines 69B-Gal4, da-Gal4, T80-Gal4 or Bx-Gal4, and the resultant phenotype analysed in adult wings. The CtB-Gal4 line (Sudarsan et al., 2002) was used to drive expression of UAS transgenes in the MpTs. The following UAS responder lines were used: UAS-GMA (Dutta et al., 2002); UAS-CD8-GFP (Lee and Luo, 1999); and UAS-*cv-c* (this study). P-element excision of l(3)06951 was performed by standard methods using Δ2,3*CyO* as the source of transposase. Germline clones were generated using the FLP-DFS technique (Chou and Perrimon, 1996) in *y w hs:FLP/w; FRT82B,* $cv\text{-}c^{M62}$*/FRT82B,* $ovo^{D}$ flies. Clones were induced with two 2-hour 37°C heat shocks, administered 24 hours apart in late 2nd and 3rd instar larvae.

### Mutagenesis and screens

#### MpT screen

The $cv\text{-}c^{M62}$ and $cv\text{-}c^{C524}$ EMS-induced alleles were generated on a multiply marked third chromosome (*rucuca*) following standard techniques. The primary screen used luminal uric acid as a marker for MpT morphology (Fig. 4O,P).

#### *cv-c*$^{1}$ screens

The $cv\text{-}c^{2}$, $cv\text{-}c^{3}$, $cv\text{-}c^{4}$, $cv\text{-}c^{5}$, $cv\text{-}c^{6}$, $cv\text{-}c^{7}$ and $cv\text{-}c^{8}$ EMS-induced alleles were generated in a F1 screen for mutations that failed to complement the recessive viable allele $cv\text{-}c^{1}$.

### Immunocytochemistry and histochemistry

Immunostaining was performed using standard techniques with antibodies against the following proteins: 22C10 (1:200), Baz (1:1500), β-galactosidase (1:10,000), Cno (1:200), Cut (1:200), E-cad (1:20), FasIII (1:20), GFP (1:1500, Abcam), p-Mad (1:2000) and Stranded-at-Second (1:500). Appropriate biotinylated secondaries were used in conjunction with the Vector Elite ABC Kit (Vector Laboratories, CA) for DAB staining. For fluorescent labelling, we used appropriate secondary antibodies conjugated either to FITC or Cy3. When required, we performed an additional amplification step using streptavidin-conjugated Cy3. *cv-c* RNA localisation was performed by in situ hybridisation using a digoxigenin-labelled antisense probe directed against the entire coding sequence of *cv-c*. GFP was visualised by antibody staining using a GFP antibody (Fig. 5E-H, Fig. 6G) or by observing GFP fluorescence in living embryos (Fig. 5K-P; Fig. 6E,F).

### Molecular biology

#### Construction of UAS-*cv-c*

The UAS-*cv-c* construct was generated by inserting the entire *cv-c* cDNA as a *Eco*RI-*Kpn*I fragment from RE02250 into the *Eco*RI-*Kpn*I sites of pUAST (Brand and Perrimon, 1993).

#### SNP mapping

SNP mapping of $cv\text{-}c^{M62}$ and $cv\text{-}c^{C524}$ was performed as previously described (Martin et al., 2001). Novel SNP loci were found by sequencing PCR-amplified intergenic DNA fragments from *rucuca*/FRT82B flies. SNP loci were scored using restriction fragment length polymorphisms (RFLPs), or allele-specific primers. The following SNP loci were used (FRT/*rucuca* alleles are given for novel SNPs): SNP-87A; SNP-88C (Martin et al., 2001) (contrary to the previous report, we find that the *rucuca* allele is A and FRT allele is G at SNP-88C); SNP-Abi [nucleotide 81776 in AE003703 (C/T, RFLP for *Xho*I)]; and SNP-NK7.1 [nucleotide 75924 in AE003704 (T/A)].

### Cuticle preparations

Embryonic cuticle preparations were performed as previously described (Hu and Castelli-Gair, 1999). Wings were dissected from adult flies in 70% ethanol and mounted in Euparal.

## Results

### New alleles of *crossveinless-c*

In a series of screens designed to isolate mutations in genes controlling morphogenesis, we obtained two EMS alleles of a gene located between the third chromosome markers *curled* and *stripe*. Further analysis using single nucleotide polymorphism (SNP) markers (Martin et al., 2001) refined the map position to 88B-88C, between SNP-NK7.1 and SNP-88C (Fig. 2A) – a region of ~116 kb that, according to the *Drosophila* genome database, contains nine predicted genes. A P-element insertion, l(3)06951, is allelic to these mutants. The *cv-c* locus also maps to chromosomal band 88C. This locus is represented by three alleles, $cv\text{-}c^{1}$, $cv\text{-}c^{c}$ and $cv\text{-}c^{M1}$, that are characterised by the loss of the posterior crossvein (PCV) and

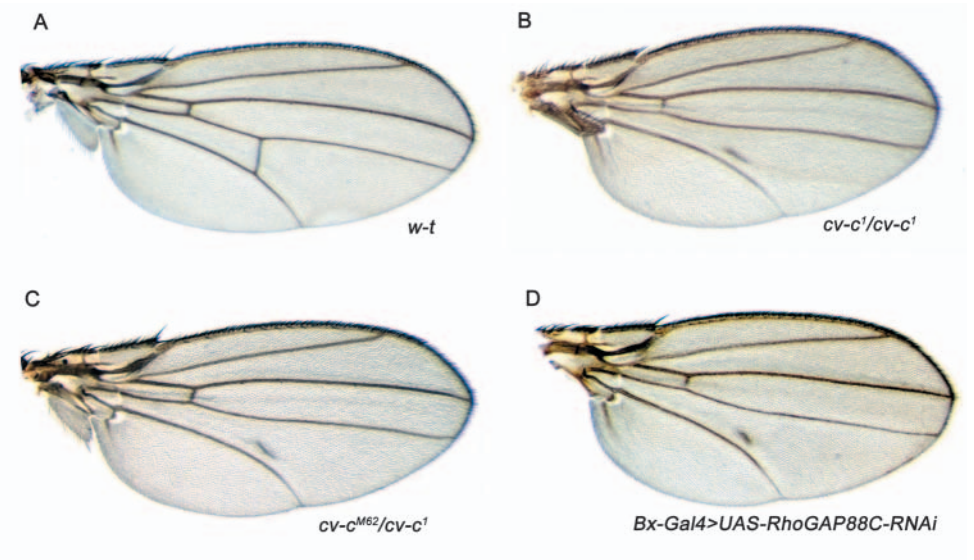


**Fig. 1.** New alleles of *cv-c*. (A) The wing of a wild-type adult fly has five longitudinal veins, and an anterior and posterior crossvein (ACV and PCV). (B) A wing from a $cv\text{-}c^{1}/cv\text{-}c^{1}$ homozygous fly. The PCV is completely absent (a small piece of vein tissue running parallel to the fifth longitudinal vein is often observed) and the ACV is detached from the fourth longitudinal vein. (C) A wing from a $cv\text{-}c^{1}/cv\text{-}c^{M62}$ fly exhibiting a PCV phenotype identical to $cv\text{-}c^{1}/cv\text{-}c^{1}$. (D) A wing in which the UAS-RhoGAP88C-dsRNA construct has been expressed throughout the developing wing disc using Bx-Gal4. The phenotypes produced are identical to $cv\text{-}c^{1}$ wings; the PCV is significantly reduced and the ACV is detached from longitudinal vein 4.

a detachment of the anterior crossvein (ACV) (compare Fig. 1A with 1B) (Diaz-Benjumea, 1990; Edmondson, 1952; Stern, 1934). Both EMS alleles and l(3)06951, when transheterozygous with each other, are lethal, but they are viable and exhibit PCV defects in trans with $cv\text{-}c^{1}$ (Fig. 1C). We isolated further alleles of *cv-c*, including a set showing embryonic lethality (see Materials and methods for screens and Table 1 for details of alleles).

## Characterisation of the *cv-c* locus

In addition to the nine predicted genes, a number of expressed sequence tags (ESTs), indicate that two other transcription units map to the *cv-c* region (EST clot numbers: 13471 and 13975). Plasmid rescue of the P-element in l(3)06951 shows that it is inserted close to SNP-88C and within the transcription unit defined by ESTs in clot 13975. However, the transcription unit defined by clot 13957 does not contain an ORF of appreciable size and we believe that the lethal mutation caused by the P-element insertion is unrelated to it (see below).

No mutants have been reported for any of the nine predicted genes flanked by our SNPs, precluding complementation analysis. However, a UAS-RNAi construct directed to RhoGAP88C (CG31319) has previously been generated (Billuart et al., 2001). We tested whether expression of this RNAi construct could recapitulate the *cv-c* phenotypes we observe. To do this, we used Gal4 driver lines that express in the developing wing throughout pupal development and are active during the period of PCV specification at 24-26 hours APF (Conley et al., 2000). The four Gal4 driver lines we tested produce a phenotype indistinguishable from the $cv\text{-}c^{1}$ phenotype (Fig. 1D). No other wing structures, including the longitudinal veins, are affected (Fig. 1D). This result contrasts with previous data reporting that expression of UAS-RhoGAP88C in the developing wing pouch (using T80-Gal4, a driver we also used) results in a reduction or absence of wing vein L2 (Billuart et al., 2001). These results suggest that *cv-c* encodes RhoGAP88C, and encouraged us to search for molecular lesions in the coding sequence of RhoGAP88C in our EMS alleles.

## Molecular characterisation of *cv-c* mutations

The *Drosophila* RhoGAP88C gene spans a region of 14 kb and contains eight exons. The BDGP database contains a single RhoGAP88C cDNA (RE02250) of 4.4 kb in length. Conceptual translation of this cDNA reveals an open reading frame of 1017 amino acids (Fig. 2B). In addition to the GAP domain, RhoGAP88C contains two other previously described domains: a sterile α motif (SAM), originally defined as a protein-protein interaction domain (Schultz et al., 1997), but more recently implicated in RNA (Aviv et al., 2003; Green et al., 2003; Kim and Bowie, 2003) and lipid membrane-binding (Barrera et al., 2003); and a lipid transfer START domain so called because it was initially isolated in the steroidogenic acute regulatory (StAR) protein (Clark et al., 1994; Sugawara et al., 1995).

Database searches identify several closely related RhoGAP proteins containing identical domain architecture to *Drosophila* RhoGAP88C (Fig. 2C). The closest related

**Table 1. Known *cv-c* alleles**

| *cv-c* allele | Mutagen | Lethal phase | Reference |
|---|---|---|---|
| $cv\text{-}c^{1}$ | Spontaneous | Viable | Stern, 1934 |
| $cv\text{-}c^{c}$ | Spontaneous | Viable | Edmondson, 1952 |
| $cv\text{-}c^{M1}$ | EMS | Unknown | Diaz-Benjumea, 1990 |
| $cv\text{-}c^{M62}$ | EMS | E/L | * |
| $cv\text{-}c^{C524}$ | EMS | E/L | * |
| $cv\text{-}c^{l(3)06951}$ | P-element | E/L | Spradling et al., 1999* |
| $cv\text{-}c^{J8}$ | Excision of $cv\text{-}c^{l(3)06951}$ | E/L | * |
| $cv\text{-}c^{J17}$ | Excision of $cv\text{-}c^{l(3)06951}$ | E/L | * |
| $cv\text{-}c^{2}$ | EMS | E/L | * |
| $cv\text{-}c^{3}$ | EMS | E/L | * |
| $cv\text{-}c^{4}$ | EMS | E/L | * |
| $cv\text{-}c^{5}$ | EMS | E/L | * |
| $cv\text{-}c^{6}$ | EMS | E/L | * |
| $cv\text{-}c^{7}$ | EMS | E/L | * |
| $cv\text{-}c^{8}$ | EMS | E/L | * |

Mutagen, lethal phase (E, embryonic; L, larval) and original reference (where available) for each allele are given.
*Alleles generated and described for the first time in this study.

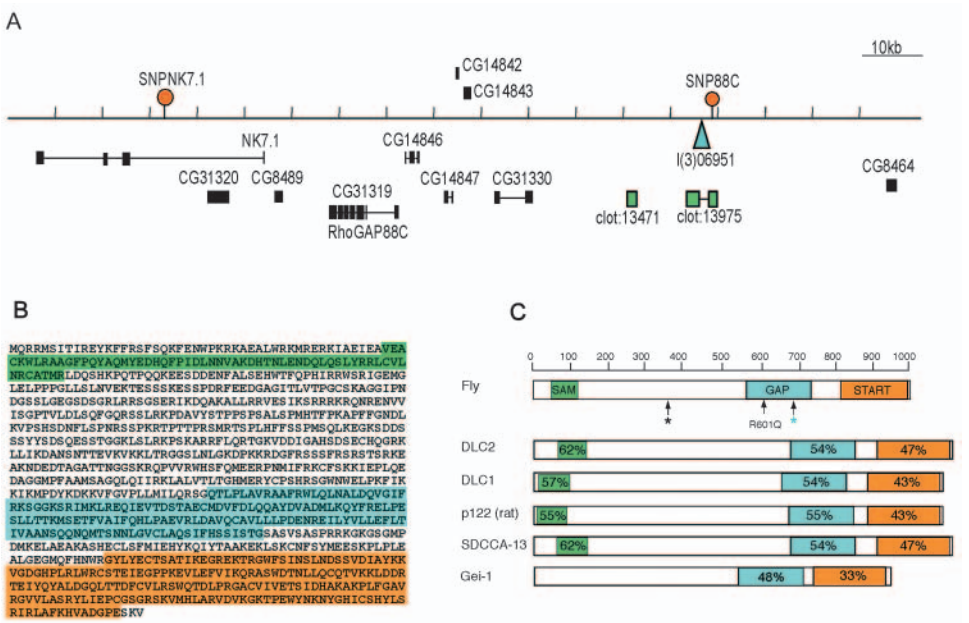


**Fig. 2.** *cv-c* encodes RhoGAP88C. (A) Genomic map depicting part of the 88B-88C interval of the third chromosome (centromere is towards the left). All known and predicted genes in the region are shown; those drawn above the line are transcribed left to right, whereas those below are transcribed right to left. Small nucleotide polymorphic (SNP) loci used for mapping are indicated with orange lollipops. The P-element inset l(3)06951 is represented by the blue triangle. Two transcription units without predicted translation products (green), are indicated by their EST clot numbers. (B) The Cv-c protein is 1017 amino acids in length and contains three evolutionarily conserved domains: the N-terminal sterile α motif (SAM) (green), the GAP domain (blue) and the C-terminal START domain (orange). (C) Comparison between fly Cv-c and its homologues: human deleted in liver cancer 1 and 2 (DLC1 and DLC2); rat p122; mouse seriologically defined in colon cancer antigen 13 (SDCCA13); and worm gut-on-exterior interacting protein 1 (GEI-1). Percentage of amino acids that are identical in fly Cv-c and in each of the homologues is shown for the SAM (green), GAP (blue) and START (orange) domains. Molecular lesions for *cv-c*$^{C524}$ [R369stop (black asterisk)], *cv-c*$^{7}$ [R601Q] and *cv-c*$^{M62}$ [Q666stop (blue asterisk)] are indicated.

vertebrate proteins are the human deleted in liver cancer 1 and 2 [DLC1 and DLC2 (STARD13 – Human Gene Nomenclature Database)], the mouse serologically defined colon cancer 13 antigen and rat p122-RhoGAP (Fig. 2C). A *C. elegans* protein, gut on exterior-interacting protein (GEI) also shares a high level of identity with *Drosophila* RhoGAP88C in the GAP and START domains, but lacks the SAM motif (Fig. 2C).

We identified molecular lesions in the coding region of three of our *cv-c* EMS alleles. Two of these, *cv-c*$^{C524}$ and *cv-c*$^{M62}$, contain nonsense mutations at amino acid positions 369 and 666, respectively, resulting in protein products truncated either before the GAP domain for *cv-c*$^{C524}$, or within it for *cv-c*$^{M62}$ (Fig. 2C). The absence of a complete GAP or START domain in either mutant product suggests they are likely to be amorphic mutations. In *cv-c*$^{7}$ (Table 1), arginine 601 is substituted for glutamine (Fig. 2C). This arginine is highly conserved at the corresponding position in RhoGAP88C homologues in other species and is also conserved in GAP proteins more distantly related to the RhoGAP family, underlining the importance of this residue for GAP function. A combination of biochemical and structural studies have shown that the conserved arginine residue projects into the active site of the GTPase and stabilises the transition state of the hydrolytic reaction (Barrett et al., 1997; Nassar et al., 1998; Rittinger et al., 1997a; Rittinger et al., 1997b; Scheffzek et al., 1997). Mutational analysis reveals that substitution of this so-called 'arginine finger' with another residue dramatically reduces the catalytic activity of the GAP protein (Leonard et al., 1998). Our finding that the arginine finger is specifically mutated in *cv-c*$^{7}$ indicates that GAP activity is central to the function of *cv-c*. Surprisingly, however, we find *cv-c*$^{7}$ homozygous embryos have consistently stronger phenotypes than either *cv-c*$^{C524}$ or *cv-c*$^{M62}$ homozygotes (see below), suggesting that *cv-c*$^{7}$ is an antimorphic allele. Our interpretation of these findings is that substitution of arginine 601 to glutamine not only abolishes the catalytic activity of *cv-c*, but also impedes the weak, intrinsic GTPase activity of its substrate. Therefore, the balance between GTP-bound and GDP-bound states of the substrate GTPase will be shifted even further towards the active, GTP-bound form in *cv-c*$^{7}$ homozygous embryos.

The P-element insertion in *cv-c*$^{l(3)06951}$ (Table 1) is ~60 kb upstream to the start of transcription (Fig. 2; see Materials and methods). The reporter activity faithfully recapitulates the endogenous expression of *cv-c* (Fig. 3; data not shown). Precise excision of the P-element reverts the lethality and *cv-c* phenotype. Both *cv-c*$^{l(3)06951}$ and the new imprecise excision alleles we have generated are homozygous lethal but are weaker than those of the amorphic mutations (Table 1; see below). In one of these excision alleles, *cv-c*$^{J17}$, *cv-c* transcripts are absent from most, but not all tissues (Fig. 3F). These results indicate that sequences controlling *cv-c* transcription reside at a considerable genomic distance from the transcription unit.

## Embryonic expression of *cv-c*

RNA in situ hybridisation to wild-type embryos shows that *cv-c* is not maternally supplied (Fig. 3A). We first detect *cv-c* RNA in stage 8 embryos in the head region, including the head mesoderm, at the tip of the cephalic furrow, in the amnioserosa, and in distinct regions of the hindgut and posterior midgut anlagen in the amnioproctodeal invagination (Fig. 3B). At stage 11, *cv-c* transcripts can be found at high levels in the tracheal pits, in the mesoderm, and at lower levels in the cells that will later become the leading edge cells during dorsal closure (Fig. 3C). Transcripts are first detected in the MpTs during germband retraction (data not shown) and accumulate to high levels in this tissue by stage 13 (Fig. 3D). At this stage, *cv-c* is also expressed in many tissues including the peripheral

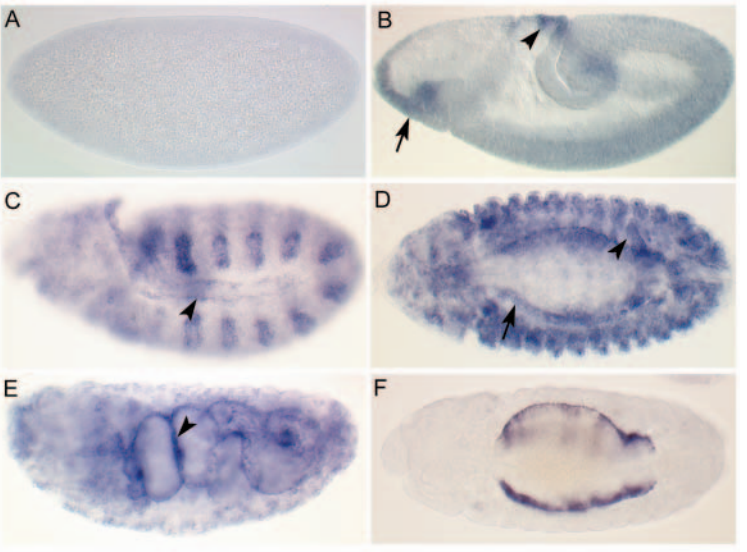


**Fig. 3.** Embryonic expression of *cv-c*. *cv-c* RNA in situ hybridisation in wild-type (A-E) or *cv-c*$^{J17}$ (F) embryos. (A) Expression is not detected in blastoderm embryos, indicating a lack of maternal contribution. (B) Expression in stage 8 embryos is seen in the head (arrow) and head mesoderm, at the tip of the cephalic furrow, in the amnioserosa (arrowhead), and within distinct regions of the hindgut and midgut primordia. (C) At stage 11, *cv-c* transcripts are detected at high levels in the tracheal pits and in the epidermal cells that will later form the leading edge cells during dorsal closure (arrowhead). (D) At stage 13, *cv-c* is expressed in many tissues, including the MpTs (arrowhead), the longitudinal visceral muscle (LVM) of the midgut (black arrow), lymph glands, peripheral nervous system and regions of the head. (E) At stage 16, the highest level of *cv-c* is in the gut visceral musculature (arrowhead). (F) *cv-c* transcripts in *cv-c*$^{J17}$ mutant embryos are detected in the LVM of the midgut but are either absent or considerably reduced in other tissues (stage 13 embryo shown). In this, and all subsequent figures, embryos are orientated with anterior towards the left.

nervous system, posterior spiracle, the somatic mesoderm, the longitudinal visceral muscles (LVM) of the midgut, the lymph gland and in the head (Fig. 3D). By stage 16, *cv-c* is expressed strongly in both the LVM and circular visceral muscles of the gut and throughout the ectoderm (Fig. 3E).

As previously discussed, *cv-c*$^{l(3)06951}$ is likely to disrupt regulatory sequences. To test this hypothesis, we examined the expression of *cv-c* in *cv-c*$^{l(3)06951}$ and the jump-out allele *cv-c*$^{J17}$. Although we were unable to detect any major differences in *cv-c* expression in *cv-c*$^{l(3)06951}$, *cv-c* expression is reduced in all tissues apart from the LVM in *cv-c*$^{J17}$ embryos (compare Fig. 3D with 3F). This confirms that the *cv-c*$^{J17}$ lesion removes *cv-c* regulatory elements.

## Mutations of *cv-c* produce defects in morphogenesis

Here, we report embryonic phenotypes associated with mutations in *cv-c*; further details of the wing phenotypes will be described elsewhere. Unless specified otherwise, we describe the mutant phenotypes of *cv-c*$^{M62}$ homozygotes, as we believe this to be an amorphic *cv-c* allele. Analysis of *cv-c* germline clones (data not shown) confirms that *cv-c* is not supplied maternally and for this reason, we used zygotic mutants for the phenotypic analysis.

The cells that contribute to the larval mouth skeleton of *Drosophila* are internalised during development in a process known as head involution (Fig. 4A). In *cv-c* mutants, cells fail to move into the embryo so that structures such as the medial tooth, the H piece and dorsal bridge remain on the surface of the embryo (Fig. 4B). *cv-c*$^{7}$ consistently shows stronger defects, in which the head does not involute normally so that the remnants of the whole head skeleton lie on the surface (Fig. 4F).

The posterior spiracle forms by invagination of surface ectodermal cells into the interior to form the spiracular chamber (Hu and Castelli-Gair, 1999) (Fig. 4C). In *cv-c* mutants, invagination of these cells is aberrant, causing defects ranging from complete failure of invagination, so that the entire internal cuticular structure (the Filzkörper) is later found on the surface, to branching of the spiracular chamber (Fig. 4D).

During dorsal closure sheets of epithelial cells on either side of the embryo move dorsally over the amnioserosa, so that their epithelial fronts meet and fuse at the dorsal midline, enclosing the embryo (Fig. 4E,G). Although embryos mutant for strong *cv-c* alleles complete dorsal closure, staining with an antibody against the apical membrane marker Stranded at second (Sas) shows that closure is delayed (compare equivalently aged embryos in Fig. 4G,H), and we frequently observe puckering of the dorsal cuticle (Fig. 4F). The phenotypes we observe do not result from abrogation of Dpp signalling, that underlies dorsal closure (see Fig. S1 in the supplementary material), suggesting defects occur in the morphogenetic movements themselves.

In wild-type embryos, the midgut becomes subdivided into four compartments by three constrictions that result from interactions between the visceral mesoderm and the underlying endoderm (Fig. 4I). The formation of these constrictions involves changes in cell shape and movement that occur without cell division (reviewed by Bienz, 1994). In *cv-c* mutant embryos, the anterior (and occasionally also the posterior) midgut constriction fails to develop (Fig. 4J). Failure of the gut constrictions is not due to defects in visceral mesoderm specification or signalling (see Fig. S1 in the supplementary material) and is therefore likely to result from defects in the normal cell movements.

In *cv-c* embryos, the MpTs form a single large cyst- or ball-like structure instead of four elongated tubules (Fig. 4K-N). This phenotype results from the failure of tubule remodelling, which normally occurs by a series of convergent extension movements, such that each tubule extends along its proximodistal axis and narrows around its circumference (compare Fig. 4K,L with 4M,N) (Denholm and Skaer, 2004). The cyst-like structure in mutants sometimes, but not always, exhibits a central lumen, which is revealed by the accumulation of secreted urates (Fig. 4O,P). In a small proportion of embryos, the distal regions of one and, occasionally, two tubules undergo normal convergent extension movements, with the distal tips finding their correct location within the body cavity (an example of this is shown in Fig. 5P).

As part of our analysis to confirm that *cv-c* encodes RhoGAP88C, we generated a UAS-RhoGAP88C construct and asked whether this could rescue the *cv-c* phenotype.

Expression of the construct in *cv-c*$^{M62}$ mutant embryos using the CtBGal4 driver, which is specific for the MpTs, rescues the tubule phenotype (Fig. 4Q), confirming that *cv-c* encodes RhoGAP88C. Furthermore, rescue of the MpT phenotype in an embryo otherwise mutant for *cv-c* demonstrates that the requirement for Cv-c activity is cell autonomous in this tissue at least. In summary, our phenotypic analysis shows that the tissues most sensitive to loss of Cv-c function are those actively

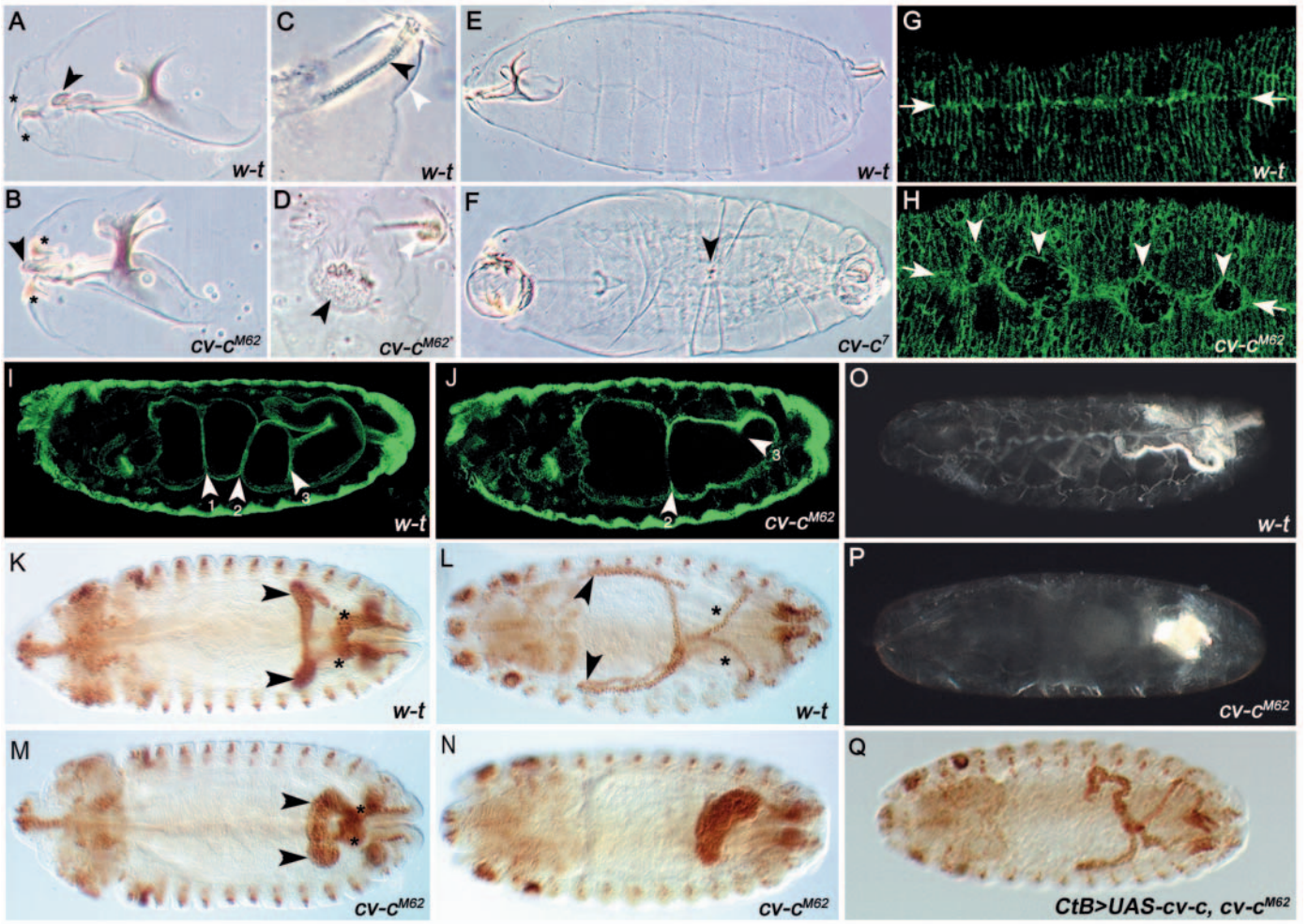


**Fig. 4.** Embryonic phenotypes of *cv-c* mutants. Cuticle preparations of late embryos viewed under phase contrast showing the head skeleton (A,B), the posterior spiracles (C,D) and the dorsal cuticle (E,F). Wild-type (A,C,E), *cv-c*$^{M62}$ homozygote (B,D) and *cv-c*$^{7}$ homozygote (F) embryos. (A) In wild-type embryos, the medial tooth occupies an internal position (arrowhead in A), whereas in 80% of *cv-c*$^{M62}$ embryos (B) the medial tooth is located on the exterior (arrowhead); the mouth hooks, which would normally be in this position, are displaced laterally (mouth hooks in A and B are indicated with asterisks). (C) A wild-type embryo with normal posterior spiracle morphology. The Filzkörper (black arrowhead), a filter formed in the internal tube connecting the spiracle to the tracheal system, is located inside the dome-like stigmatophore (white arrowhead). (D) In 28% of *cv-c*$^{M62}$ posterior spiracles analysed, the cells that form the Filzkörper do not invaginate and instead form a 'lawn' on the exterior (black arrowhead). In 67% of posterior spiracles analysed, the Filzkörper cells invaginate but do so aberrantly such that the final Filzkörper is branched (white arrowhead). (E) A wild-type embryo with normal dorsal cuticle morphology. (F) A *cv-c*$^{7}$ embryo showing puckering of the dorsal cuticle (arrowhead). (G,H) Stage 15 embryos stained with anti-SAS showing the latter stages of dorsal closure. (G) The leading edge cells of the lateral epidermis zip up along the dorsal midline (arrows) during stage 15 in wild-type embryos. (H) In *cv-c* mutant embryos, this process is delayed and less orderly. Arrows and arrowheads indicate the dorsal midline and regions of delayed closure. (I,J) Midgut morphology of stage 16 embryos visualised with the Fas3 antibody (which marks the visceral muscle overlying the midgut) in wild-type (I) or *cv-c*$^{M62}$ (J) embryos. The anterior-most constriction (1) does not occur in *cv-c*$^{M62}$ embryos, and the posterior-most constriction (3) is variably affected. (K-P) MpT morphology is disrupted in *cv-c* embryos. (K-N) MpT development visualised by staining with the Cut antibody, in wild-type (K,L) and *cv-c*$^{M62}$ embryos (M,N). Defects in *cv-c*$^{M62}$ embryos become obvious by stage 13 as the MpTs start their convergent extension movements (compare K with M). By stage 16, the wild-type MpTs have formed four long, thin tubules, positioned invariantly within the body cavity (L), whereas the *cv-c*$^{M62}$ MpTs have coalesced into a large cyst-like ball (N). Anterior (arrowhead) and posterior (asterisk) tubules are marked where they can be distinguished. (O,P) Nitrogenous waste products are excreted as urates that precipitate to form uric acid crystals in the acidic environment of the tubule lumen; these can be visualised in stage 17 embryos using polarised light. (O) A wild-type embryo, with normal posterior tubule morphology. (P) A *cv-c*$^{M62}$ homozygous embryo in which the MpTs have formed a cyst-like ball; urates are excreted into a large central lumen. (Q) A stage 16 *cv-c* mutant embryo in which wild-type *cv-c* has been expressed in the MpTs. The MpT phenotype is partially rescued. Embryos are shown from lateral (A-E,I,J,O,P) or dorsal (F-H,K-N,Q) perspectives.

undergoing morphogenetic movement or remodelling. We propose that the *cv-c* gene product functions autonomously to perform a fundamental role in the control of morphogenesis of multiple tissues.

### *cv-c* is required to organise the actin cytoskeleton

The morphogenetic defects we observe could result from alterations in cell polarity or cell shape through cytoskeletal reorganisation. In order to distinguish between these, we first analysed both planar and apicobasal polarity of cells in *cv-c* embryos. We chose to examine planar polarity in epidermal cells during dorsal closure because it is not known whether the MpTs exhibit planar polarity. To do this, we visualised the redistribution of Canoe (Cno). In wild-type embryos, Cno is expressed at the cell cortex of leading edge cells, but as dorsal closure proceeds it clears from sites of apposition with the amnioserosa and refines to distinct puncta where adjacent epidermal cells meet (Kaltschmidt et al., 2002) (Fig. 5A,C). This redistribution depends on the planar cell polarity pathway (Kaltschmidt et al., 2002). We find that this redistribution of Cno occurs normally in *cv-c* mutant embryos (Fig. 5B,D), indicating that planar polarity is not disrupted in the absence of Cv-c activity. We next examined whether *cv-c* tubule cells have normal apicobasal polarity. Using CD8-GFP to label the entire membrane of MpT cells and staining for the apical membrane marker Bazooka (Baz) reveals that apicobasal polarity is established normally and maintained in *cv-c* 'tubules' until the end of embryogenesis (Fig. 5E-H). In addition, the presence and position of the adherens junction marker dE-Cadherin relative to apical markers such as Sas are normal in mutant tubule cells (Fig. 5I,J).

We then focussed our attention on the actin cytoskeleton. To do this, we made use of the UAS-GMA construct, which encodes the actin-binding region of moesin fused to GFP and provides a faithful readout of filamentous actin localisation (Dutta et al., 2002). Using the CtB-Gal4 driver, we expressed UAS-GMA in the MpTs throughout embryonic development. In wild-type embryos at stage 13, F-actin is found localised to the cell cortex of all tubule cells and is particularly enriched at the apical (luminal surface) (Fig. 5K). A similar distribution

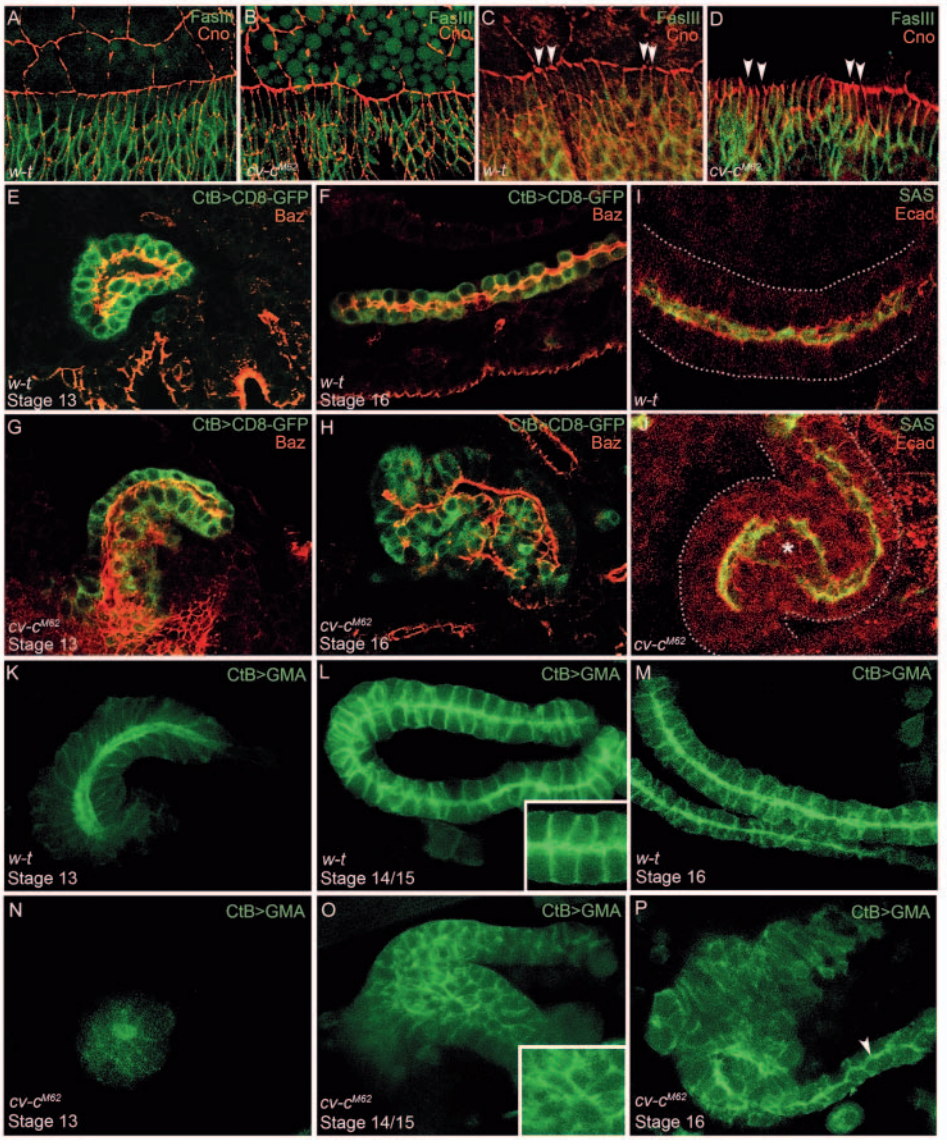


**Fig. 5.** Cellular basis of the *cv-c* phenotype. (A-D) Planar polarity of the dorsal epidermis is unaffected in *cv-c* embryos. In wild-type embryos, the Cno protein (red) is initially expressed around the entire cell cortex, but later clears from sites of apposition with the amnioserosa and refines to distinct puncta (arrowheads), where adjacent epidermal cells meet. This pattern is seen in *cv-c* embryos (B,D) as in wild type (A,C). (E-H) Apicobasal polarity in the MpTs is unaffected in *cv-c* embryos. Embryos in which UAS-CD8-GFP was driven in the MpTs to label the entire membrane (green) were also stained with Baz (red) to mark the apical membrane. Wild-type (E,F) and *cv-c* (G,H) at stages 13 and 16. In *cv-c* tubules, apicobasal polarity is established and maintained. (I,J) The adherens junctions appear unaffected in *cv-c* embryos. Wild-type (I) and *cv-c* (J) stage 14 embryos stained with Sas (green) and Ecad (red). The level of expression and the relative position of the two markers in *cv-c* MpTs is identical to wild type. Asterisk in J indicates the lumen. (K-P) The level and distribution of cortical F-actin is disrupted in the MpTs of *cv-c* embryos. (K) In wild-type stage 13 MpTs, F-actin is localised to both the lateral and, in particular, the apical cell cortices. (L,M) F-actin continues to accumulate at the lateral and apical cell cortices; at stage 14/15, it appears compact and in close apposition to the plasma membrane (inset in L). (N) In stage 13 *cv-c* mutant MpTs, F-actin fails to accumulate in the cortex, remaining diffuse in the cytoplasm. (O) In stage 14 *cv-c* mutant MpTs, F-actin remains perinuclear, showing little concentration in the subcortex (inset in O). (P) In a small number of *cv-c* mutant MpTs, the distal end of the tubule elongates (arrowhead); in these cases, cortical F-actin is similar to wild type (M) seen at stage 16.

of F-actin is maintained throughout the remainder of embryogenesis (Fig. 5L,M). F-actin distribution is more diffuse in stage 13 *cv-c* mutant embryos, and although it is present around the cell cortex, its levels here are significantly lower than in wild-type embryos (Fig. 5N). Similarly, apical accumulation of actin is either absent or, at best, very weak (Fig. 5N). Although F-actin becomes localised to the cell cortex in later stages of development, its distribution is less compact than in wild type and diffuse staining throughout the cytoplasm suggests that attachment of the subcortical actin network to the membrane is disrupted (Fig. 5O,P; compare inset in L with inset in O). Although apical accumulation of F-actin is never observed in *cv-c* cystic MpTs, those in which the distal end does become tubular possess weak apical F-actin accumulation at the luminal membrane (Fig. 5P, arrowhead). These data show that Cv-c is required to regulate the spatial organisation of F-actin in tubule cells during morphogenesis. Furthermore, apical accumulation of F-actin, which is largely absent in *cv-c* tubules, is crucial for the maintenance of tubular integrity; in its absence the MpTs collapse to form cyst-like sack structures.

## Gain of function analyses suggest that Cv-c stabilises membrane/actin associations

In order to analyse the GOF phenotype, we overexpressed Cv-c in the MpTs throughout embryogenesis. Tubules in which Cv-c is ectopically expressed are significantly shorter in length and fatter around their circumference, suggesting that elevated Cv-c activity also causes defects in convergent extension movements (data not shown). The most obvious phenotype we observe, however, affects the tip cell, a specialised cell that protrudes from the distal end of each of the four tubules (Fig. 6A) (Skaer, 1989). The length of the tip cell stalk is ~7 μm in both wild-type tubules and in the tubules of *cv-c* loss-of-function embryos (Fig. 6B,C). However, when Cv-c is overexpressed, the stalk length can increase to over 50 μm (Fig. 6D) [average length=24 μm ($n$=56)]. Analysis using 22C10, which labels the tip cell membrane, as well as observations of F-actin, reveal that the extended stalk is associated with underlying F-actin (Fig. 6D,F). Staining for Sas reveals that the stalk is an extension of the basolateral, rather than apical membrane (Fig. 6G). We reasoned that if the normal function of Cv-c is to downregulate the activity of RhoGTPases, then overexpression of a dominant-negative RhoGTPase might be expected to produce a similar phenotype. This is indeed the case: ectopic expression of the dominant-negative Rho1 construct UAS-Rho.N19 (but not the dominant-negative Rac1 construct UAS-Rac1.N17 – see below) resulted in an increase in tip cell stalk similar to the phenotype in *cv-c* overexpression (Fig. 6H) [average length, 15 μm ($n$=22)]. These data, taken together with the loss-of-function analysis described above, are consistent with a role for Cv-c in regulating or stabilising links between the cell membrane and the cortical actin cytoskeleton. Furthermore, in agreement with the genetic interaction experiments described below, these data further suggest that this function for Cv-c, in the MpTs at least, is mediated at the level of Rho1 and not Rac1 activity (see below).

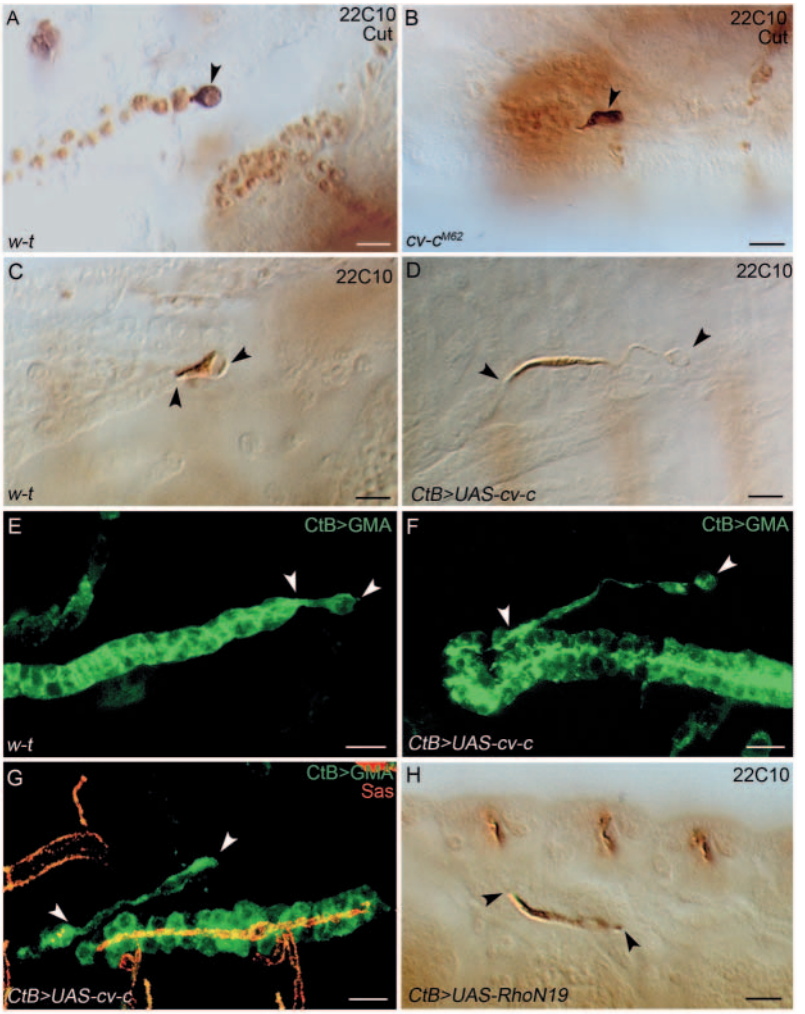


**Fig. 6.** Overexpression of *cv-c* produces long actin-filled cellular extensions. (A,B) Wild-type (A) and *cv-c*$^{M62}$ (B) stage 16 embryos stained with anti-Cut (light brown) to label the MpT nuclei and 22C10 (dark brown) to label the tip cell. The tip cell is present and has a normal morphology in *cv-c*$^{M62}$ homozygotes. (C,D) The tip cell stalk of a wild-type embryo is ~7 μm (C) but increases dramatically in length in embryos in which UAS-*cv-c* has been expressed in the tubule using CtB-Gal4; in many cases, the length of the stalk exceeds 50 μm (D) ($n$=56). (E,F) Stage 16 embryos expressing UAS-GMA in the MpTs to label F-actin (green), either in the absence of *cv-c* overexpression (E) or when *cv-c* is overexpressed (F); the extended tip cell stalk is associated with F-actin. (G) CtB-Gal4>UAS-GMA;UAS-*cv-c* embryo co-stained for GFP (green) and the apical membrane marker Sas (red, overlap in yellow). The tip cell stalk does not stain for Sas, indicating that the extension is of basolateral membrane. (H) 22C10 staining of a stage 16 embryo in which a dominant-negative Rho1 construct (UAS-RhoN19) has been overexpressed in the tubules; the tip cell stalk is extended ($n$=22). In all figures, arrowheads indicate the extent of the tip cell. Scale bars: 10 μm.

## Genetic interactions between *cv-c* and RhoGTPases

RhoGAPs normally function to stimulate the intrinsic GTP

hydrolysing capacity of the GTPases, thereby converting them to the inactive GDP-bound form. Thus, the phenotypes we observe in the absence of Cv-c function are likely to be caused by elevated activities of the cognate GTPase substrate(s) of Cv-c. Such relationships can be tested by genetic interactions; a reduction in the activity of a substrate GTPase would rescue the *cv-c* phenotype, while an increase in GTPase activity would enhance it. To identify the substrate(s) of Cv-c, we analysed genetic interactions between *cv-c* and candidate GTPases for which mutants are available. Embryos homozygous for *cv-c*$^{M62}$ and homozygous or hemizygous for mutations in the GTPases *Rho1*, *Rac1*, *Rac2*, *Mtl* and *Cdc42* were analysed for both the MpT and embryonic cuticle phenotypes.

Removal of any of the Rac candidates, *Rac1*, *Rac2* or *Mtl*, and reduction or removal of *Cdc42* failed to modify the *cv-c*$^{M62}$ phenotype in the MpTs. By contrast, 50% of *cv-c*$^{M62}$ mutant embryos additionally homozygous for *Rho1*$^{72R}$ ($n$=48) and 20% of *cv-c*$^{M62}$ mutant embryos heterozygous for *Rho1*$^{72R}$ ($n$=56) had a phenotype significantly less severe than that of the *cv-c*$^{M62}$ homozygote alone. The MpTs of doubly mutant embryos undergo convergent extension movements to some extent (compare Fig. 7A,B and 7A′,B′), such that they resemble weaker alleles of *cv-c* (data not shown). These data strongly suggest that Rho1 is a substrate for Cv-c in the MpTs.

We next examined genetic interations in the embryonic epidermis. Dorsal closure defects occur in 82% of embryos doubly mutant for *Rac1* and *Rac2* ($n$=46) (this study, Fig. 7C) (Hakeda-Suzuki et al., 2002). However, if *Rac1,Rac2* embryos are additionally mutant for *cv-c*$^{M62}$, 37% of these embryos are rescued ($n$=44) (Fig. 7D), indicating that Rac GTPases are substrates for Cv-c during dorsal closure.

The posterior spiracle phenotype in *cv-c* embryos was not suppressed by any of the RhoGTPase mutants, possibly because maternal contribution of the substrate GTPase is sufficient to provide full activity in this tissue. However, we unexpectedly find that embryos mutant for both *Rac1* and *Rac2* do not decrease, but enhance the *cv-c*$^{M62}$ posterior spiracle phenotype (compare Fig. 7E with 7F). One possible explanation for this interaction comes from observations in cell culture, where it has been shown that Rac activity downregulates Rho activation (Nimnual et al., 2003; Sander et al., 1999). If Rac normally functions to inhibit Rho in the posterior spiracle, then loss of Rac and Cv-c together, would lead to hyperactivity in Rho1 and this would lead to the enhancement of the *cv-c* phenotype. In support of this, we see *cv-c*-like posterior spiracle phenotypes with low penetrance in *Rac1 Rac2* embryos (data not shown).

In summary, our data from these genetic analyses in the embryo indicate that *cv-c* interacts with *Rho1*, *Rac1* and *Rac2*. Furthermore, these data suggest that interactions between Cv-c and its substrates might be regulated in a tissue-specific manner.

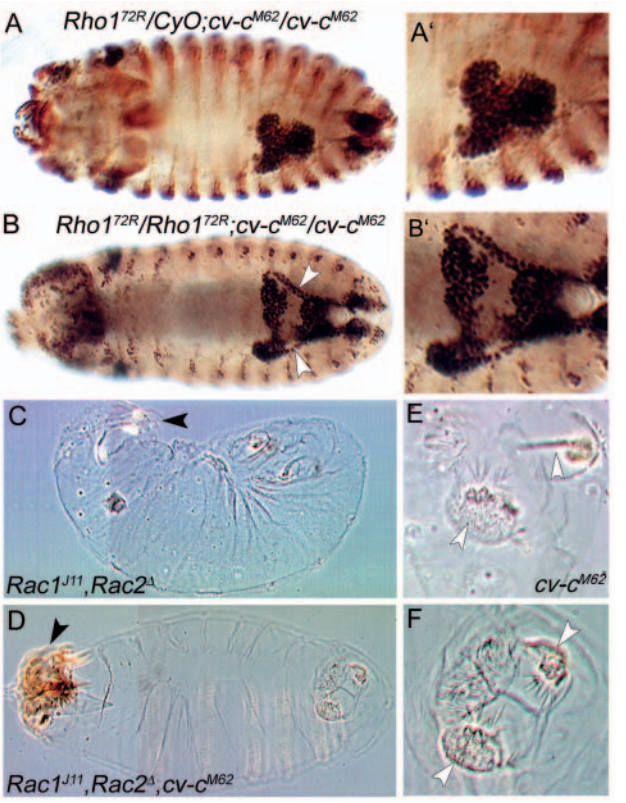


**Fig. 7.** Genetic interaction with Rho-family GTPases. (A-B′) Stage 16 embryos stained with an antibody against Cut (dark brown) or β-galactosidase (light brown). (A) *Rho1*$^{72R}$*/CyOwg-LacZ; cv-c*$^{M62}$*/cv-c*$^{M62}$ embryo exhibiting the typical *cv-c*$^{M62}$ MpT phenotype. (A′) Higher magnification of MpTs shown in A. (B) A much less severe MpT phenotype is seen in *Rho1*$^{72R}$*/Rho1*$^{72R}$*; cv-c*$^{M62}$*/cv-c*$^{M62}$ embryos ($n$=48), in which normal tubulogenesis often takes place. Arrowheads in B indicate elongated anterior MpTs. (B′) Higher magnification of MpTs shown in B. (C-F) Cuticle preparations of late embryos. (C) *Rac1*$^{J11}$*,Rac2*$^{\Delta}$ mutant embryos show abnormal head involution (black arrowhead), germband retraction and strong dorsal closure phenotypes in 82% of the embryos ($n$=46). (D) In *Rac1*$^{J11}$*,Rac2*$^{\Delta}$*,cv-c*$^{M62}$ mutant embryos, head involution (arrowhead), germband retraction and dorsal closure phenotypes are less severe; the dorsal closure phenotype is rescued in 37% of embryos ($n$=44). (E,F) *cv-c*$^{M62}$ posterior spiracle phenotypes are enhanced in a *Rac1*$^{J11}$*,Rac2*$^{\Delta}$ background. (E) *cv-c*$^{M62}$ homozygote showing variable penetrance of the posterior spiracle phenotype (arrowheads). (F) *Rac1*$^{J11}$*,Rac2*$^{\Delta}$*,cv-c*$^{M62}$ showing complete penetrance of the posterior spiracle phenotype (arrowheads). In 71% of *Rac1,Rac2,cv-c*$^{M62}$ embryos, posterior spiracle invagination fails and the spiracles remain on the exterior (compared with 28% in *cv-c*$^{M62}$ embryos).

## Discussion

In three independent screens to detect mutations affecting tissue morphogenesis we have isolated novel alleles of *cv-c*. Phenotypic analyses show that Cv-c function is required in embryonic tissues for specific morphogenetic events: in the gut for normal midgut morphogenesis and for MpT elongation; and in the epidermis for the invagination of the posterior spiracle, head involution and ordered dorsal closure. We show that *cv-c* encodes RhoGAP88C, a regulator of Rho-family GTPases, and demonstrate that it interacts genetically with *Rho* and *Rac* GTPases, possibly in a tissue-specific manner. We go on to show that defects in MpT morphogenesis in *cv-c* mutants correlate with defects in the organisation of the subcortical actin cytoskeleton. Finally, we show that overexpression of *cv-c* leads to stable actin-filled membrane extensions

The common feature linking the morphogenetic processes in which *cv-c* activity is required is the coordinated reorganisation

of large groups of cells during tissue remodelling. Such processes involve choreographed cell movements as well as alterations in cell shape. We have focused our attention on the role of Cv-c in the morphogenesis of the MpTs as they undergo convergent extension movements. In contrast to cell polarity, which is relatively normal in *cv-c* mutant embryos, we find that the organisation of the actin cytoskeleton is aberrant. We show that the normal strong subcortical accumulation of F-actin is lost in *cv-c* mutant MpTs. In particular, the striking concentration of F-actin on the luminal membrane at the onset of tubule elongation fails.

How do these defects in the actin cytoskeleton relate to the MpT morphogenetic phenotype? By a process of convergent extension, starting at stage 13 and continuing until stage 16, the MpT cells remodel from short fat tubes with 10-12 cells surrounding the lumen to long thin tubes with only two cells encircling the lumen. The convergent extension movements in the MpTs are likely to occur in a manner similar to those described in the epidermis during germband extension, whereby a coordinated reorganisation of cell partners drives a change in tissue dimension (Bertet et al., 2004). Central to this reorganisation is the remodelling of zonula adherens junctions (ZAs), which are progressively disassembled as ZAs between new cell partners are formed (Bertet et al., 2004). Remodelling of the actin cytoskeleton is thought to drive these changes, both to facilitate alterations in cell shape and finally to stabilise the new junctional configuration. We suggest that the defects in the actin cytoskeleton observed in *cv-c* tubules perturbs the cell rearrangements that underlie convergent extension movements required during tubule elongation. As the MpT phenotype becomes progressively more severe during the period when cell rearrangement normally occurs, we suggest that it is the coordination of cell reorganisation rather than cell intercalation per se that is defective. In addition, morphogenesis of the MpTs requires the maintenance of a tubular structure and this also fails in *cv-c* mutants. It is likely that the accumulation of actin at the luminal membrane is required both to remodel cell-cell associations and to retain the integrity of the lumen. We therefore propose that Cv-c plays an important regulatory role to ensure that the actin cytoskeleton is properly remodelled during tubule morphogenesis. Furthermore, as *cv-c* is required in multiple tissues, we predict that *cv-c* is reiteratively used during development in the regulation of actin cytoskeletal remodelling during morphogenesis.

It seems likely that Cv-c acts to orchestrate the actin cytoskeleton via the direct regulation of RhoGTPase activity; our finding that *cv-c*$^{7}$ is defective in a specific crucial residue required for GAP enzymatic activity provides strong support for this hypothesis. Although our genetic interaction experiments highlight potential substrates and furthermore suggest the possibility that substrates might be regulated in a tissue-specific manner, additional biochemical analyses will be necessary to confirm this.

Cv-c function appears to be evolutionarily conserved. The rat and human *cv-c* homologues, p122 and DLC2 respectively, have been shown to inhibit Rho-mediated assembly of actin stress fibres when overexpressed in cell culture (Ching et al., 2003; Nagaraja and Kandpal, 2004; Sekimata et al., 1999). Furthermore, the *C. elegans cv-c* homologue, GEI-1, is thought to provide a molecular link with the actin assembly machinery. GEI-1, was isolated as a binding partner of GEX-2, one of a group of interacting proteins that localise to the plasma membrane and are required for the process of ventral enclosure, a morphogenetic event similar to dorsal closure in the fly (Soto et al., 2002; Tsuboi et al., 2002). The recent molecular characterisation of GEX-1 as a WAVE-family protein (M. Soto, personal communication) sheds light on the function of these proteins in morphogenesis. Proteins of the WAVE-family are known to relay signals from Rho-family GTPases to the actin cytoskeleton, possibly by permitting the assembly of multi-protein complexes, including components that act to nucleate actin [such as Arp2/3- and actin-binding proteins, GTPase proteins, GAPs and GEFs (Hussain et al., 2001; Scita et al., 1999; Soderling et al., 2002; Welch and Mullins, 2002)]. Thus, a molecular link exists between the Gex proteins, GTPases, their regulators and the actin cytoskeleton. Cv-c and its homologues may provide GAP activity within this large multi-protein complex, contributing to dynamic regulation of the actin cytoskeleton. For these reasons, it will be interesting to determine the relationship between Cv-c and the Gex homologues in the fly, Sra1/Gex2 and Kette/Gex3, and the fly SCAR/WAVE (Hummel et al., 2000; Kitamura et al., 1996; Kunda et al., 2003; Schenck et al., 2003; Zallen et al., 2002).

Our demonstration that overexpression of *cv-c* is sufficient to induce stable membrane extensions supported by F-actin suggests that Cv-c acts to coordinate or stabilise interactions that occur between the plasma membrane and the actin cytoskeleton. The Cv-c protein contains two domains implicated in lipid membrane binding, the START and SAM domains (Barrera et al., 2003; Hanada et al., 2003; Romanowski et al., 2002; Tsujishita and Hurley, 2000), suggesting that Cv-c localises to a membrane domain. This would place Cv-c in an ideal position to regulate an interaction between the plasma membrane and the actin cytoskeleton. There is compelling evidence that moesin is required to organise the cortical actin network which it does, at least in part, by linking the actin cytoskeleton to the plasma membrane (for reviews, see Bretscher et al., 2002; Gautreau et al., 2002; Polesello and Payre, 2004). Given that moesin has been shown to antagonise Rho1 by altering its activation state (Speck et al., 2003), it will also be interesting to examine the requirement of Cv-c for moesin function.

We thank David Strutt and Richard Fehon for fly stocks, and Doug Cavener, Eli Knust and Peter ten Dijke for the Sas, Baz and pMad antibodies. We also thank Naomi Foster, Denise Tan and Emma Swinnerton for their contribution to the project, and Paloma Martín Fernández for her technical assistance. We are grateful to members of our laboratory for many helpful discussions and comments on the manuscript. R.P.R. thanks Trudi Schüpbach, in whose laboratory the screens for mutations allelic to *cv-c*$^{1}$ were performed. This work was supported by the Wellcome Trust (H.S., J.C.-G.H., B.D. and S.B.); The Royal Society (J.C.-G.H. and R.P.R.); a grant from the Dirección General de Investigación, Ministerio de Ciencia y Tecnología (BMC2003-05056); and an Institutional grant from Fundación Ramón Areces to the Centro de Biología Molecular Severo Ochoa (M.R.-G.).

## Supplementary material

Supplementary material for this article is available at
http://dev.biologists.org/cgi/content/full/132/10/2389/DC1

## References


**Aviv, T., Lin, Z., Lau, S., Rendl, L. M., Sicheri, F. and Smibert, C. A.** (2003). The RNA-binding SAM domain of Smaug defines a new family of post-transcriptional regulators. *Nat. Struct. Biol.* **10**, 614-621.

**Barrera, F. N., Poveda, J. A., Gonzalez-Ros, J. M. and Neira, J. L.** (2003). Binding of the C-terminal sterile alpha motif (SAM) domain of human p73 to lipid membranes. *J. Biol. Chem.* **278**, 46878-46885.

**Barrett, T., Xiao, B., Dodson, E. J., Dodson, G., Ludbrook, S. B., Nurmahomed, K., Gamblin, S. J., Musacchio, A., Smerdon, S. J. and Eccleston, J. F.** (1997). The structure of the GTPase-activating domain from p50rhoGAP. *Nature* **385**, 458-461.

**Bernards, A.** (2003). GAPs galore! A survey of putative Ras superfamily GTPase activating proteins in man and Drosophila. *Biochim. Biophys. Acta.* **1603**, 47-82.

**Bertet, C., Sulak, L. and Lecuit, T.** (2004). Myosin-dependent junction remodelling controls planar cell intercalation and axis elongation. *Nature* **429**, 667-671.

**Bienz, M.** (1994). Homeotic genes and positional signalling in the Drosophila viscera. *Trends Genet.* **10**, 22-26.

**Billuart, P., Winter, C. G., Maresh, A., Zhao, X. and Luo, L.** (2001). Regulating axon branch stability: the role of p190 RhoGAP in repressing a retraction signaling pathway. *Cell* **107**, 195-207.

**Boettner, B. and van Aelst, L.** (2002). The role of Rho GTPases in disease development. *Gene* **286**, 155-174.

**Brand, A. H. and Perrimon, N.** (1993). Targeted gene expression as a means of altering cell fates and generating dominant phenotypes. *Development* **118**, 401-415.

**Bretscher, A., Edwards, K. and Fehon, R. G.** (2002). ERM proteins and merlin: integrators at the cell cortex. *Nat. Rev. Mol. Cell Biol.* **3**, 586-599.

**Ching, Y. P., Wong, C. M., Chan, S. F., Leung, T. H., Ng, D. C., Jin, D. Y. and Ng, I. O.** (2003). Deleted in liver cancer (DLC) 2 encodes a RhoGAP protein with growth suppressor function and is underexpressed in hepatocellular carcinoma. *J. Biol. Chem.* **278**, 10824-10830.

**Chou, T. B. and Perrimon, N.** (1996). The autosomal FLP-DFS technique for generating germline mosaics in Drosophila melanogaster. *Genetics* **144**, 1673-1679.

**Clark, B. J., Wells, J., King, S. R. and Stocco, D. M.** (1994). The purification, cloning, and expression of a novel luteinizing hormone-induced mitochondrial protein in MA-10 mouse Leydig tumor cells. Characterization of the steroidogenic acute regulatory protein (StAR). *J. Biol. Chem.* **269**, 28314-28322.

**Conley, C. A., Silburn, R., Singer, M. A., Ralston, A., Rohwer-Nutter, D., Olson, D. J., Gelbart, W. and Blair, S. S.** (2000). Crossveinless 2 contains cysteine-rich domains and is required for high levels of BMP-like activity during the formation of the cross veins in Drosophila. *Development* **127**, 3947-3959.

**Denholm, B. and Skaer, H.** (2004). Development of Malpighian tubules in Insects. In *Comprehensive Molecular Insect Science*, Vol. 2 (ed. L. I. Gilbert, S. Gill and K. Iatrou), pp. 291-314. Oxford, UK: Elsevier.

**Diaz-Benjumea, F. J. and Garcia-Bellido, A.** (1990). Genetic analysis of the wing vein pattern of Drosophila. *Roux's Arch. Develop. Biol.* **198**, 336-354.

**Dutta, D., Bloor, J. W., Ruiz-Gomez, M., VijayRaghavan, K. and Kiehart, D. P.** (2002). Real-time imaging of morphogenetic movements in Drosophila using Gal4-UAS-driven expression of GFP fused to the actin-binding domain of moesin. *Genesis* **34**, 146-151.

**Edmondson, M.** (1952). New mutants report. *Dros. Inf. Serv.* **26**, 60-62.

**Etienne-Manneville, S. and Hall, A.** (2002). Rho GTPases in cell biology. *Nature* **420**, 629-635.

**Gautreau, A., Louvard, D. and Arpin, M.** (2002). ERM proteins and NF2 tumor suppressor: the Yin and Yang of cortical actin organization and cell growth signaling. *Curr. Opin. Cell Biol.* **14**, 104-109.

**Green, J. B., Gardner, C. D., Wharton, R. P. and Aggarwal, A. K.** (2003). RNA recognition via the SAM domain of Smaug. *Mol. Cell* **11**, 1537-1548.

**Guichard, A., Bergeret, E. and Griffin-Shea, R.** (1997). Overexpression of RnRacGAP in Drosophila melanogaster deregulates cytoskeletal organisation in cellularising embryos and induces discrete imaginal phenotypes. *Mech. Dev.* **61**, 49-62.

**Hakeda-Suzuki, S., Ng, J., Tzu, J., Dietzl, G., Sun, Y., Harms, M., Nardine, T., Luo, L. and Dickson, B. J.** (2002). Rac function and regulation during Drosophila development. *Nature* **416**, 438-442.

**Hall, A.** (1998). Rho GTPases and the actin cytoskeleton. *Science* **279**, 509-514.

**Hanada, K., Kumagai, K., Yasuda, S., Miura, Y., Kawano, M., Fukasawa, M. and Nishijima, M.** (2003). Molecular machinery for non-vesicular trafficking of ceramide. *Nature* **426**, 803-809.

**Hu, N. and Castelli-Gair, J.** (1999). Study of the posterior spiracles of Drosophila as a model to understand the genetic and cellular mechanisms controlling morphogenesis. *Dev. Biol.* **214**, 197-210.

**Hummel, T., Leifker, K. and Klambt, C.** (2000). The Drosophila HEM-2/NAP1 homolog KETTE controls axonal pathfinding and cytoskeletal organization. *Genes Dev.* **14**, 863-873.

**Hussain, N. K., Jenna, S., Glogauer, M., Quinn, C. C., Wasiak, S., Guipponi, M., Antonarakis, S. E., Kay, B. K., Stossel, T. P., Lamarche-Vane, N. et al.** (2001). Endocytic protein intersectin-l regulates actin assembly via Cdc42 and N-WASP. *Nat. Cell Biol.* **3**, 927-932.

**Jaffe, A. B. and Hall, A.** (2002). Rho GTPases in transformation and metastasis. *Adv. Cancer Res.* **84**, 57-80.

**Kaltschmidt, J. A., Lawrence, N., Morel, V., Balayo, T., Fernandez, B. G., Pelissier, A., Jacinto, A. and Martinez Arias, A.** (2002). Planar polarity and actin dynamics in the epidermis of Drosophila. *Nat. Cell Biol.* **4**, 937-944.

**Kim, C. A. and Bowie, J. U.** (2003). SAM domains: uniform structure, diversity of function. *Trends Biochem. Sci.* **28**, 625-628.

**Kitamura, T., Kitamura, Y., Yonezawa, K., Totty, N. F., Gout, I., Hara, K., Waterfield, M. D., Sakaue, M., Ogawa, W. and Kasuga, M.** (1996). Molecular cloning of p125Nap1, a protein that associates with an SH3 domain of Nck. *Biochem. Biophys. Res. Commun.* **219**, 509-514.

**Kunda, P., Craig, G., Dominguez, V. and Baum, B.** (2003). Abi, Sra1, and Kette control the stability and localization of SCAR/WAVE to regulate the formation of actin-based protrusions. *Curr. Biol.* **13**, 1867-1875.

**Lee, T. and Luo, L.** (1999). Mosaic analysis with a repressible cell marker for studies of gene function in neuronal morphogenesis. *Neuron* **22**, 451-461.

**Leonard, D. A., Lin, R., Cerione, R. A. and Manor, D.** (1998). Biochemical studies of the mechanism of action of the Cdc42-GTPase-activating protein. *J. Biol. Chem.* **273**, 16210-16215.

**Lundström, A., Gallio, M., Englund, C., Steneberg, P., Hemphala, J., Aspenstrom, P., Keleman, K., Falileeva, L., Dickson, B. J. and Samakovlis, C.** (2004). Vilse, a conserved Rac/Cdc42 GAP mediating Robo repulsion in tracheal cells and axons. *Genes Dev.* **18**, 2161-2171.

**Martin, S. G., Dobi, K. C. and St Johnston, D.** (2001). A rapid method to map mutations in Drosophila. *Genome Biol.* **2**, RESEARCH0036.

**Nagaraja, G. M. and Kandpal, R. P.** (2004). Chromosome 13q12 encoded Rho GTPase activating protein suppresses growth of breast carcinoma cells, and yeast two-hybrid screen shows its interaction with several proteins. *Biochem. Biophys. Res. Commun.* **313**, 654-665.

**Nassar, N., Hoffman, G. R., Manor, D., Clardy, J. C. and Cerione, R. A.** (1998). Structures of Cdc42 bound to the active and catalytically compromised forms of Cdc42GAP. *Nat. Struct. Biol.* **5**, 1047-1052.

**Nimnual, A. S., Taylor, L. J. and Bar-Sagi, D.** (2003). Redox-dependent downregulation of Rho by Rac. *Nat. Cell Biol.* **5**, 236-241.

**Nobes, C. D. and Hall, A.** (1995a). Rho, rac and cdc42 GTPases: regulators of actin structures, cell adhesion and motility. *Biochem. Soc. Trans.* **23**, 456-459.

**Nobes, C. D. and Hall, A.** (1995b). Rho, rac, and cdc42 GTPases regulate the assembly of multimolecular focal complexes associated with actin stress fibers, lamellipodia, and filopodia. *Cell* **81**, 53-62.

**Peck, J., Douglas, G. T., Wu, C. H. and Burbelo, P. D.** (2002). Human RhoGAP domain-containing proteins: structure, function and evolutionary relationships. *FEBS Lett.* **528**, 27-34.

**Polesello, C. and Payre, F.** (2004). Small is beautiful: what flies tell us about ERM protein function in development. *Trends Cell Biol.* **14**, 294-302.

**Raymond, K., Bergeret, E., Dagher, M. C., Breton, R., Griffin-Shea, R. and Fauvarque, M. O.** (2001). The Rac GTPase-activating protein RotundRacGAP interferes with Drac1 and Dcdc42 signalling in Drosophila melanogaster. *J. Biol. Chem.* **276**, 35909-35916.

**Rittinger, K., Walker, P. A., Eccleston, J. F., Nurmahomed, K., Owen, D., Laue, E., Gamblin, S. J. and Smerdon, S. J.** (1997a). Crystal structure of a small G protein in complex with the GTPase-activating protein rhoGAP. *Nature* **388**, 693-697.

**Rittinger, K., Walker, P. A., Eccleston, J. F., Smerdon, S. J. and Gamblin, S. J.** (1997b). Structure at 1.65 A of RhoA and its GTPase-activating protein in complex with a transition-state analogue. *Nature* **389**, 758-762.

**Romanowski, M. J., Soccio, R. E., Breslow, J. L. and Burley, S. K.** (2002). Crystal structure of the Mus musculus cholesterol-regulated START protein 4 (StarD4) containing a StAR-related lipid transfer domain. *Proc. Natl. Acad. Sci. USA* **99**, 6949-6954.

**Sagnier, T., Grienenberger, A., Mariol, M., Berenger, H., Pradel, J. and Graba, Y.** (2000). Dynamic expression of d-CdGAPr, a novel Drosophila melanogaster gene encoding a GTPase activating protein. *Mech. Dev.* **94**, 267-270.

**Sander, E. E., ten Klooster, J. P., van Delft, S., van der Kammen, R. A. and Collard, J. G.** (1999). Rac downregulates Rho activity: reciprocal balance between both GTPases determines cellular morphology and migratory behavior. *J. Cell Biol.* **147**, 1009-1022.

**Scheffzek, K., Ahmadian, M. R., Kabsch, W., Wiesmuller, L., Lautwein, A., Schmitz, F. and Wittinghofer, A.** (1997). The Ras-RasGAP complex: structural basis for GTPase activation and its loss in oncogenic Ras mutants. *Science* **277**, 333-338.

**Schenck, A., Bardoni, B., Langmann, C., Harden, N., Mandel, J. L. and Giangrande, A.** (2003). CYFIP/Sra-1 controls neuronal connectivity in Drosophila and links the Rac1 GTPase pathway to the fragile X protein. *Neuron* **38**, 887-898.

**Schultz, J., Ponting, C. P., Hofmann, K. and Bork, P.** (1997). SAM as a protein interaction domain involved in developmental regulation. *Protein Sci.* **6**, 249-253.

**Scita, G., Nordstrom, J., Carbone, R., Tenca, P., Giardina, G., Gutkind, S., Bjarnegard, M., Betsholtz, C. and di Fiore, P. P.** (1999). EPS8 and E3B1 transduce signals from Ras to Rac. *Nature* **401**, 290-293.

**Sekimata, M., Kabuyama, Y., Emori, Y. and Homma, Y.** (1999). Morphological changes and detachment of adherent cells induced by p122, a GTPase-activating protein for Rho. *J. Biol. Chem.* **274**, 17757-17762.

**Settleman, J.** (2001). Rac 'n Rho: the music that shapes a developing embryo. *Dev. Cell* **1**, 321-331.

**Skaer, H.** (1989). Cell division in Malpighian tubule development in D. melanogaster is regulated by a single tip cell. *Nature* **342**, 566-569.

**Soderling, S. H., Binns, K. L., Wayman, G. A., Davee, S. M., Ong, S. H., Pawson, T. and Scott, J. D.** (2002). The WRP component of the WAVE-1 complex attenuates Rac-mediated signalling. *Nat. Cell Biol.* **4**, 970-975.

**Sotillos, S. and Campuzano, S.** (2000). DRacGAP, a novel Drosophila gene, inhibits EGFR/Ras signalling in the developing imaginal wing disc. *Development* **127**, 5427-5438.

**Soto, M. C., Qadota, H., Kasuya, K., Inoue, M., Tsuboi, D., Mello, C. C. and Kaibuchi, K.** (2002). The GEX-2 and GEX-3 proteins are required for tissue morphogenesis and cell migrations in C. elegans. *Genes Dev*. **16**, 620-632.

**Speck, O., Hughes, S. C., Noren, N. K., Kulikauskas, R. M. and Fehon, R. G.** (2003). Moesin functions antagonistically to the Rho pathway to maintain epithelial integrity. *Nature* **421**, 83-87.

**Spradling, A. C., Stern, D., Beaton, A., Rhem, E. J., Laverty, T., Mozden, N., Misra, S. and Rubin, G. M.** (1999). The Berkeley Drosophila Genome Project gene disruption project: Single P-element insertions mutating 25% of vital Drosophila genes. *Genetics* **153**, 135-177.

**Stern, C.** (1934). New mutants report. *Dros. Inf. Serv.* **1**, 35-36.

**Sudarsan, V., Pasalodos-Sanchez, S., Wan, S., Gampel, A. and Skaer, H.** (2002). A genetic hierarchy establishes mitogenic signalling and mitotic competence in the renal tubules of Drosophila. *Development* **129**, 935-944.

**Sugawara, T., Holt, J. A., Driscoll, D., Strauss, J. F., 3rd, Lin, D., Miller, W. L., Patterson, D., Clancy, K. P., Hart, I. M., Clark, B. J. et al.** (1995). Human steroidogenic acute regulatory protein: functional activity in COS-1 cells, tissue-specific expression, and mapping of the structural gene to 8p11.2 and a pseudogene to chromosome 13. *Proc. Natl. Acad. Sci. USA* **92**, 4778-4782.

**Tsuboi, D., Qadota, H., Kasuya, K., Amano, M. and Kaibuchi, K.** (2002). Isolation of the interacting molecules with GEX-3 by a novel functional screening. *Biochem. Biophys. Res. Commun.* **292**, 697-701.

**Tsujishita, Y. and Hurley, J. H.** (2000). Structure and lipid transport mechanism of a StAR-related domain. *Nat. Struct. Biol.* **7**, 408-414.

**Van Aelst, L. and Symons, M.** (2002). Role of Rho family GTPases in epithelial morphogenesis. *Genes Dev.* **16**, 1032-1054.

**Welch, M. D. and Mullins, R. D.** (2002). Cellular control of actin nucleation. *Annu. Rev. Cell Dev. Biol.* **18**, 247-288.

**Zallen, J. A., Cohen, Y., Hudson, A. M., Cooley, L., Wieschaus, E. and Schejter, E. D.** (2002). SCAR is a primary regulator of Arp2/3-dependent morphological events in Drosophila. *J. Cell Biol.* **156**, 689-701.